Fischer carbene mediated covalent grafting of a peptide nucleic acid on gold surfaces and IR optical detection of DNA hybridization with a transition metalcarbonyl label

Pratima Srivastava, Mahsa Ghasemi, Namrata Ray, Amitabha Sarkar, Jana Kocabova, Stepanka Lachmanova, Magdalena Hromadova, Souhir Boujday, Silvia Cauteruccio, Emanuela Licandro, et al.

Fischer carbene mediated covalent grafting of a peptide nucleic acid on gold surfaces and IR optical detection of DNA hybridization with a transition metalcarbonyl label

Pratima Srivastava[a]srivastavapratima13@yahoo.fr, Mahsa Ghasemi[a]mghasemi78@yahoo.com, Namrata Ray[b]nr.2610@gmail.com, Amitabha Sarkar[b]ocas@iacs.res.in, Jana Kocabova[c]jana.kocabova@jh-inst.cas.cz, Stepanka Lachmanova[c]stepanka.lachmanova@jh-inst.cas.cz, Magdalena Hromadova[c]magdalena.hromadova@jh-inst.cas.cz, Souhir Boujday[d]souhir.boujday@upmc.fr, Silvia Cauteruccio[e]Emanuela.licandro@unini.it, Pramod Thakare[e]silvia.cauteruccio@unimi.it, Emanuela Licandro[e]pramod.thakare@unimi.it, Céline Fosse[f]Celine.fosse@chimie-paristech.fr, Michèle Salmain[a*]Michele.salmain@upmc.fr

[a]Sorbonne Universités, UMPC Univ Paris 06, CNRS, Institut Parisien de Chimie Moléculaire (IPCM), UMR 8232, 4 place Jussieu, F-75005 Paris, France.

[b]Indian Association for the Cultivation of Science, Department of Organic Chemistry, 700032 Kolkatta, India.

[c]J. Heyrovsky Institute of Physical Chemistry, Academy of Sciences of the Czech Republic, Dolejskova 3, CZ-18223 Prague, Czech Republic.

[d]Sorbonne Universités, UMPC Univ Paris 06, CNRS, Laboratoire de Réactivité de Surface (LRS), UMR 7197, 4 place Jussieu, F-75005 Paris, France.

[e]Università degli Studi di Milano, Dipartimento di Chimica, via C. Golgi 19, I-20133 Milano, Italy.

[f]PSL Research University, Chimie ParisTech, CNRS, Institut de Recherche de Chimie Paris, F-75005 Paris, France.

* Correspondence author: Tel.: +33 144276732

Graphical abstract

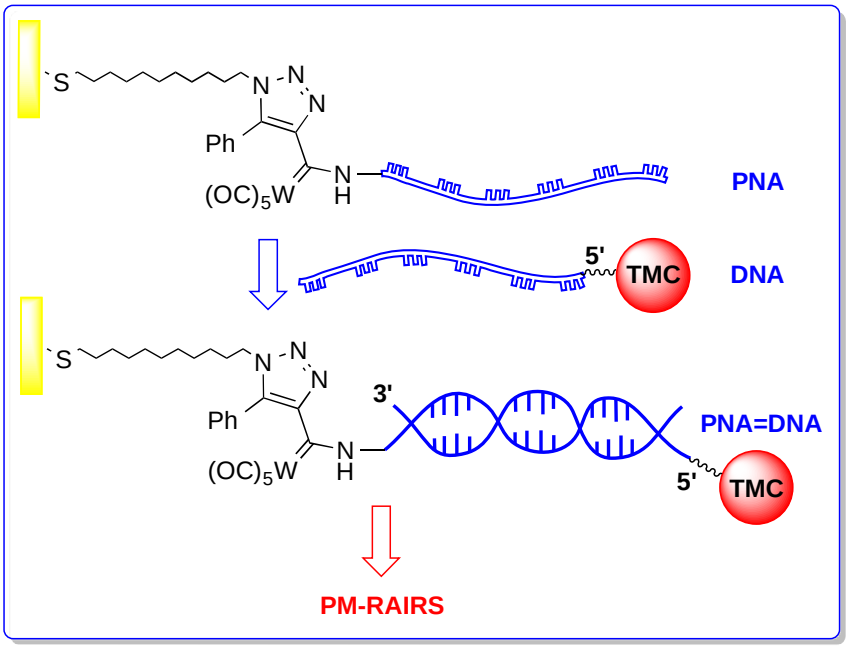

Highlights

- Covalent anchoring of PNA to gold-coated surfaces covered with amine-reactive groups
- Analysis of thin films by complementary surface analytical techniques
- Mid-IR optical transduction of hybridization using a transition metalcarbonyl probe

Abstract

Amine-reactive surfaces comprising N-hydroxysuccinimide ester groups as well as much more unusual Fischer alkoxymetallocarbene groups were generated on gold-coated surfaces via self-assembled monolayers of carboxy- and azido-terminated thiolates, respectively. These functions were further used to immobilize homothymine peptide nucleic acid (PNA) decamer in a covalent fashion involving the primary amine located at its N-terminus. These stepwise processes were monitored by polarization modulation reflection – absorption infrared spectroscopy (PM-RAIRS) that gave useful information on the molecular composition of the organic layers. PNA grafting and hybridization with complementary DNA strand were successfully transduced by quartz crystal microbalance (QCM) measurements. Unfortunately, attempts to transduce the hybridization optically by IR in a label-free fashion were inconclusive. Therefore we undertook to introduce an IR reporter group, namely a transition metalcarbonyl (TMC) entity at the 5' terminus of complementary DNA. Evidence for the formation of PNA-DNA heteroduplex was brought by the presence of ν(C≡O) bands in the 2000 cm^{-1} region of the IR spectrum of the gold surface owing to the metalcarbonyl label.

Keywords

Peptide nucleic acid; self-assembled monolayer; genosensor; Fischer-type carbene complex; azide-alkyne cycloaddition; PM-RAIRS

1. Introduction

The construction of thin films of biomolecules on solid supports is one of the key steps in the design of biosensors [1]. Immobilization methods should allow controlling both the density and orientation of the adsorbed molecules while maintaining their bioactivity, i.e. their ability to selectively recognize and bind the target species. When dealing with gold surfaces, one of the most useful strategies is to generate self-assembled monolayers (SAMs)[1] of thiol-containing molecules carrying a functional end group. Thanks to the high affinity of sulfur for gold, control over orientation of the molecules and consequently of the functional groups is readily exerted and highly ordered and densely packed monomolecular films can be generated by a simple chemisorption process [2]. In a second step, the functional group located at the solid / liquid interface is used to attach the bio(macro)molecule, for instance via a covalent link so as to generate a stable biorecognition layer [3-5]. ~~Tailoring of the density of biomolecules can be conveniently achieved by generating mixed SAMs where the reactive groups are dispersed within a matrix of inert thiols~~. In this matter, one of the most attractive and versatile approaches relies on copper-catalyzed cycloaddition reactions ("click chemistry") between azide- or alkyne-terminated SAMs and azide- or alkyne-containing biomolecules such as DNA, peptides, proteins and carbohydrates [6-10]

In this field, we have devised original two-step strategies to generate amine-reactive SAMs at the surface of glass (SiO_2) or gold substrates. They are based on the well-known reaction of Fischer metalloalkoxycarbene complexes with amines that affords metalloaminocarbenes in high yield. These alkoxycarbene entities can be introduced either by Ru-catalyzed cross-metathesis reaction between alkene-terminated SAM and alkene containing Fischer carbene [11] or by copper-free 1,3-dipolar cycloaddition reaction between azide-terminated SAM and an alkynyl Fischer carbene [12-14]. These strategies were successfully applied to covalently immobilize Protein A and staphylococcal enterotoxin A (SEA) onto gold or glass surfaces by aminolysis involving some of the pendant amino groups of both proteins. This kind of surface chemistry makes the biomolecule immobilization process easy to assess by IR spectroscopy, owing to the spectral signature of the metallocarbene entities in the 2000 cm^{-1} spectral range. Moreover these proteins were shown to retain their ability to bind their respective target, i.e. rabbit IgG and anti-SEA antibody.

Peptide nucleic acids (PNAs) are synthetic DNA mimics in which the deoxyribose-phosphodiester backbone is replaced by 2-aminoethyl glycine linkage [15]. PNAs display unique features with respect to DNA: they are achiral, neutral polymers with high chemical and biochemical stability [16]. They hybridize to complementary DNA according to the Watson-Crick base-pairing rules and DNA-PNA hybrids are more stable than the corresponding DNA-DNA ones. Consequently, PNAs display a better mismatch discrimination

[1] List of abbreviations used : AFM, atomic force microscopy ; DIPEA, diisopropylethylamine ; ~~HATU, 1-[Bis(dimethylamino)methylene]-1*H*-1,2,3-triazolo[4,5-*b*]pyridinium 3-oxid hexafluorophosphate;~~ HFIP, Hexafluoroisopropanol ; MBHA, 4-methylbenzylhydrylamine; MUA, 11-mercaptoundecanoic acid; ~~NMP, N-methyl-2-pyrrolidone~~; NS, nanoshaving; PNA, peptide nucleic acid; ODN, oligonucleotide; PBS, phosphate buffered saline; PM-RAIRS, polarization-modulation reflection-absorption infrared spectroscopy; QCM-D, quartz crystal microbalance with dissipation; SAM, self-assembled monolayer; SEA, staphylococcal enterotoxin A; ssDNA, single strand DNA; TEA, triethylamine; ~~TFA, trifluoroacetic acid; TFMSA, trifluoromethylsulfonic acid;~~ TM, tapping mode; TMC, transition metalcarbonyl; TSTU, N,N,N',N'-tetramethyl-O-(N-succinimidyl)uronium tetrafluoroborate

that the corresponding DNAs [17]. For all of these reasons, PNA stands as a valuable alternative to DNA to build up genosensors [18, 19].

Herein we demonstrate that an alkoxycarbene-terminated SAM on gold is a useful platform to generate a dense film of PNA strands. Moreover, the orientation of the strands with respect to the surface is ensured by selective reaction of its N-terminus. Furthermore, hybridization of complementary ssDNA was transduced gravimetrically with a quartz crystal microbalance as well as optically by infrared spectroscopy using a transition metalcarbonyl (TMC) marker attached to the 5'-end of target DNA.

2. Material and methods

2.1. Materials

Oligonucleotides dA_{10} and dA_{10}-5'NH_2 (high purity salt free grade) were purchased from Eurofins MWG Operon. Toluene and DMF were dried over molecular sieves. All other solvents were used as received. Bis(11-azidoundecyl)disulfide [14] and phenylacetylenylethoxycarbene pentacarbonyl tungsten(0) [13, 20] were synthesized according to the literature. 11-Mercaptoundecanoic acid (MUA), 11-bromoundecanethiol, N,N,N',N'-tetramethyl-O-(N-succinimidyl)uronium tetrafluoroborate (TSTU) and *N*,*N*-diisopropylethylamine (DIPEA) were purchased from Aldrich. Gold-coated glass slides consisting of a 250 nm-thick layer of gold on a 1.5 nm-thick chromium sublayer deposited on borosilicate glass (11x11 mm, Arrandee, Werther, Germany) were annealed by brief passage in a butane flame until a red glow appeared at the edges, dipped in ethanol 15 min and finally dried under argon stream. Gold-coated quartz sensors with a nominal resonance frequency of 5 MHz were purchased from Lot-Oriel. Before use they were cleaned by ethanol and dried with a stream of nitrogen.

2.2. Instrumentation

Transmission and ATR-IR spectra were recorded on a Tensor 27 spectrometer (Bruker). PM-RAIRS spectra were recorded on a Nexus FT-IR spectrometer (Thermo-Nicolet). The external beam was focused on the sample with a mirror at an incident angle of ca. 80°. The incident beam was modulated between p and s polarizations using a ZnSe grid polarizer and a photoelastic modulator at 37 MHz (PEM90, Hindus instruments). The light reflected from the sample was focused on a nitrogen-cooled MCT detector. All the spectra reported below were recorded at 8 cm^{-1} resolution by co-adding 64 or 128 scans.

Piezoelectric measurements were performed in flow-through mode with a quartz crystal microbalance with dissipation monitoring QCM-D (E4 model, Q-sense AB, Sweden) at 22±0.1 °C. Solutions were flowed at 50 µl.min^{-1} over the sensing area with a peristaltic pump. Mass uptakes Δm were calculated with the Sauerbrey equation (1) using the frequency at the fifth harmonics.

$$\Delta F = -\times\frac{\Delta m}{C_f} \quad (1)$$

where C_f = 17.7 ng.cm^{-2}.Hz^{-1} is the mass sensitivity factor at F = 5 MHz and N (=1, 3, 5, 7 …) is the overtone number.

Atomic force microscopy (AFM) images were obtained in the tapping mode (TM) with Nanoscope 5500 SPM microscope (Agilent Technologies, USA) and type II MAClevers

cantilevers (nominal resonant frequency 75 kHz, force constant 2.8 N/m, Agilent Technologies, USA). Nanoshaving (NS) was used to obtain information on the thickness of the corresponding layers on the gold substrate. At least five different areas of the sample surface were scrutinized by the AFM NS method and the adlayer thickness was obtained from statistical analysis of the cross-sections before and after nanoshaving. All images were visualized and analyzed using the Gwyddion 2.35 software (Czech Metrology Institute, Brno, Czech Republic) [21].

Contact angle measurements were performed using the sessile drop (static) technique with a Digidrop GBX goniometer equipped with a CCD video camera and a horizontal light source to illuminate the liquid droplet. Ultrapure water droplets (0.4 µl) were deposited on the surface using a fine, blunt syringe needle at room temperature (20 ± 2°C). The drop images were fitted using the Young-Laplace equation with the Visiodrop software. Contact angles given here are the average of at least 7 measurements. Reproducibility was within 0.5°.

2.3. Methods

2.3.1. Formation of azide-terminated SAMs

Freshly annealed gold substrates were dipped into a 1 mM solution of bis(11-azidoundecyl)disulfide in EtOH for 60 h at room temperature, washed with EtOH and dried in a flow of argon. Alternatively, samples were dipped in a degassed 1 mM solution of 11-bromoundecanethiol at 60°C under argon for 23 h in an air-tight container, then rinsed copiously with pure ethanol to remove any physisorbed residues, further incubated in pure ethanol at 60°C for 6 h to improve the formation of compact self-assembled monolayers, finally washed with pure ethanol and dried under argon stream. They were then dipped in a saturated solution of NaN_3 in DMF for 3 days, washed with DMF, ethanol and dried under argon stream.

2.3.2. Formation of amine-reactive SAMs

Azide-terminated SAMs were treated with a 1 or 10 mM solution of Fischer metallocarbene in dry toluene for 4 h at 50°C and copiously washed with toluene to remove any physisorbed complex from the surface. The carboxy-terminated SAM formed by chemisorption of MUA was treated with a freshly prepared 50 mM solution of TSTU and DIPEA in DMF for 1 h. Samples were transferred into a vial containing DMF and sonicated for 3 min and finally dried as above.

2.3.3. Immobilization of PNA

For IR and AFM measurements, gold-coated glass substrates were covered with a PNA solution (5 or 2.4 µM; borate buffer pH 8.5; 150 µl) for 1 h, washed with water and dried as above. For QCM measurements, a PNA solution (12 µM; carbonate buffer pH 8.5) was flown over the sensor chip for 18 min then flushed with carbonate buffer.

2.3.4. Hybridization studies

For IR and AFM measurements, a solution of dA_{10} or dA_{10}-5'NH$[Co_2(CO)_6]$ (5 or 12 µM in PBS; 150 µl) was dropped onto the slides and incubated for 1 h at RT. The slides were washed with water and dried as above. For QCM measurement, a solution of dA_{10} (12 µM in PBS) was flown over the sensor chip for 15 min and flushed with PBS.

3. Results and discussion

3.1. Immobilization of PNA on gold-coated glass slides

The homothymine PNA decamer (**PNA t_{10}**, Fig. 1) was synthesized by standard manual Boc-based chemistry using MBHA resin loaded with the homothymine monomer at the 20 μmol scale. The final sequence was purified by reverse phase HPLC, and its purity (up to 98%) and identity was confirmed by HPLC and MALDI-TOF MS analysis.

Formation of monolayers of PNA strands onto gold surfaces has been previously achieved by introducing a cysteine residue (i.e. a sulfhydryl functionality) at one extremity of the sequence (generally the pseudo 5' end or N-terminus) during solid-phase synthesis followed by direct chemisorption to the surface [22-36]. Alternatively, PNA strands have been immobilized by affinity via the biotin / avidin system [35, 37-40] or by conjugation to carboxyl-terminated SAMs [41, 42]. We have also shown that appending four lysine residues to the C-terminus of the homothymine decamer enabled the formation of a dense and stable layer of PNA molecules at the surface of a gold electrode nanostructured with gold nanoparticles by formation of Au-N bonds [43, 44] For this work, we devised a more general immobilization strategy making use of the single primary amine function located at the pseudo 5' terminus (NH_2-terminus) of the PNA molecule and of an appropriate bifunctional linker able to connect the **PNA t_{10}** to the Au surface [36] (Scheme 1).

This immobilization route is based on the build up of a self-assembled monolayer (SAM) of amine-reactive, Fischer-type alkoxymetallocarbene entities [12-14, 45]. These functionalities are known to swiftly react with primary amines [46, 47] including those carried by proteins [48, 49] to afford stable aminocarbenes. To form such an amine-reactive surface, a SAM of azido-terminated alkylthiolate molecules was firstly generated at the gold surface by chemisorption of bis(11-azidoundecyl)disulfide (A in Scheme 1). ~~Given the length of the alkyl chain, a well-ordered and densely packed monolayer should be formed~~. Then ethoxycarbene units were installed by Huisgen-type, 1,3-dipolar cycloaddition reaction between the surface azido groups and phenylacetylenylethoxycarbene pentacarbonyl tungsten in toluene. This bifunctional compound displays a marked electrophilic character at the carbenic carbon and contains an activated carbon-carbon triple bond which enables the 1,3-cycloaddition reaction with azides to be performed without Cu(I) catalyst [50]. The whole process was monitored by PM-RAIRS analysis of the gold surface (Figure 2). Band assignments are gathered in Table 1.

Chemisorption of the azidothiol was evidenced by the presence of a characteristic band at 2090 cm^{-1} assigned to the stretching vibration mode of the N=N(+)=N(-) group. Subsequent treatment with the metallocarbene complex led to a dramatic change of the surface IR spectrum with the disappearance of the 2090 cm^{-1} band and the appearance of 3 bands at 2067, 1982 and 1940 cm^{-1} assigned to the stretching modes ν(C≡O) of the 5 CO ligands of the $W(CO)_5$ entity [46]. The position of these bands together with the disappearance of the 2090 cm^{-1} band and the presence of a broad band centered at 1639 cm^{-1} and assigned to ν(C=C) of the triazole ring attests for the conversion of the surface azido groups into triazole groups by the cycloaddition reaction with the metallocarbene alkyne complex. No attempt

to quantify the extent of azide conversion was perfomed at this stage, owing to the relatively poor intensity of the $\nu(N_3)$ band on the IR spectrum of the azido-terminated SAM.

With the amine-reactive surface in hand, we proceeded to the immobilization of PNA. A drop of PNA solution in basic buffer (to regenerate the free amine group from the protonated one present in the PNA molecule) was spotted on the surface of the gold-coated glass slide and incubation was pursued for 1 h. After copious washing with buffer and water and drying, the gold-coated slide was analyzed again by PM-RAIRS (Fig. 2). The most intense $\nu(C{\equiv}O)$ band (A_1+E modes) was significantly blue-shifted by 8 cm^{-1}. This behavior is typical of the conversion of an alkoxy- to an aminocarbene [46]. Simultaneously, a broad unsymmetrical band centered at 1651 cm^{-1} was observed. We assigned this band to the overlapping of the amide I band originating from the polyamide backbone of PNA since the amide I band of pure PNA (which is also the most prominent band on its ATR-IR spectrum) occurs at 1668 cm^{-1} (fig. 2, right box, spectrum A). The second most prominent group of bands in the 1200 cm^{-1} region of the IR spectrum of the PNA t_{10} was not observed on the surface because it is owned by the CF_3COO^- counterion of the PNA sample that is probably washed away during the chemisorption process.

Contact angles were measured on gold-coated surfaces by the sessile drop technique at each step of functionalization (Table 2). Chemisorption of azidothiolate SAM resulted in a contact angle of ca. 71° which is close to the value of 77° previously reported in the literature [51]. After reaction with the alkynyl Fischer metallocarbene (step B), a slight decrease of the contact angle was observed. After exposure to PNA (step C), the contact angle dropped down in agreement with the more polar but uncharged nature of PNA.

Figure 3 shows a tapping mode AFM image of the adsorbed PNA t_{10} film (Scheme 1, step C), which indicates that the adsorbate was deposited in a grain-like fashion. A very similar surface morphology was observed for shorter PNA-ferrocene self-assembled monolayers by Paul *et al.* [52]. Roughness factor of the film is R = 1.14, which represents the ratio of real surface area of 4.55 μm^2 to 4 μm^2, expected for a smooth surface. The roughness average R_a was equal to 12.2 ± 2.4 nm. Both parameters describing surface morphology were obtained by the Gwyddion 2.35 software. In order to gain more useful information on the PNA t_{10} film thickness, a part of the image area was subjected to AFM nanoshaving, which enabled complete removal of the adsorbate from the selected gold surface area by a constant force in the contact mode AFM regime. The surface was imaged again in the tapping AFM mode (Fig. S1 of the supplementary material) and the adlayer thickness was evaluated from the profiles of the corresponding AFM images before and after nanoshaving (Fig. S2). Statistical analysis of the average height of the removed material in the case of matching profiles (Fig. S3 A) or of the differences between the adsorbate-covered and cleaned regions (Fig. S3 B) gives the most probable film thickness value [53-55]. It should be stressed that rough surfaces are not good candidates for the film thickness analysis through NS AFM due to difficulties in the finding of the matching profiles. Also more than one value of film thickness may be obtained due to a multilayer character of the film. In the case of the adsorbed PNA t_{10} film the average layer thickness of 33.9 ± 5.7 nm was obtained, which exceeds by several times the extended length of the PNA t_{10} molecular structure depicted in Scheme 1C, which should be approximately 7 nm, based on the molecular model calculated by the Spartan'08 (WAVEFUNCTION, Inc., U.S.A.) software.

For comparison, we set up a more "classical" route to create amine-reactive groups on the surface of gold chips. A SAM of carboxyl-terminated thiolate was first formed by chemisorption of MUA. Then the carboxyl groups were converted into N-hydroxysuccinimide esters by reaction with TSTU in the presence of DIPEA [56] which conveniently replaces the mixture of EDC and NHS owing to the allergen properties of EDC [57]. Each step of functionalization was again monitored by PM-RAIRS (Fig. 4).

Upon exposure to 1 mM MUA solution in EtOH, 2 ν(C-H) bands were observed in the 3000 cm^{-1} spectral range as well as two intense bands centered at 1628 and 1427 cm^{-1} assigned to the asymmetric and symmetric stretching vibrations of the COO^- group, respectively. After treatment with TSTU, a new set of bands appeared at 1817 and 1743 cm^{-1}, which are typical of the N-hydroxysuccinimide entity [56-59]. Further exposure to a solution of PNA in basic buffer resulted in the disappearance of the 1817 cm^{-1} band and the appearance of a broad band centered at 1659 cm^{-1} that could be due to the overlapping of the amide I band of PNA with the previous 1639 cm^{-1} band as well as a band at 1740 cm^{-1} which may be assigned to the C=O stretching of the thymine nucleobases [60].

The sequence of chemical reactions up to treatment with TSTU was repeated with a gold-coated quartz crystal sensor. The sensor was mounted in the QCM-D and carbonate buffer was flowed over the sensor until frequency stabilization. Then a 12 µM solution of PNA in the same buffer was injected and frequency and dissipation were monitored continuously. At frequency stabilization, PNA was flushed with carbonate buffer. The evolution of the frequency shift as a function of time is shown in fig. 5. It shows a clear negative shift upon injection of the PNA solution with stabilization occurring within 1200 s. In the meantime, the variation of dissipation ΔD was insignificant (< $1x10^{-6}$), indicating that the newly formed film of PNA molecules was rigid and the observed ΔF only reflected mass uptake without viscoelastic contribution [61]. Therefore the surface concentration of PNA chemisorbed to the quartz chip calculated from the Sauerbrey equation taking 17.7 $ng.cm^{-2}.Hz^{-1}$ as sensitivity factor was equal to 48 ± 5 $ng.cm^{-2}$, i.e. 1.1 ± $0.1x10^{13}$ $molecules.cm^{-2}$. For comparison, direct chemisorption of thiolated PNA probes onto gold electrodes resulted in surface densities of $6x10^{13}$ [22], $1.3x10^{13}$ [27], $3.3±0.3x10^{13}$ [62] or $1.7x10^{13}$ $molecules.cm^{-2}$ [26]. According to the literature [52], one molecule of PNA in the standing-up orientation occupies an area of 0.49 nm^2 so that a full monolayer comprises $1.3x10^{14}$ $molecules.cm^{-2}$, whereas one 10-mer PNA in the lying down orientation occupies an area of 3.4 nm^2, i.e. 2.9 x 10^{13} $molecules.cm^{-2}$ for a full monolayer. According to these calculations, the percentage of coverage in PNA molecules ranged between ca. 10 and 30% of a full monolayer depending on its orientation with respect to the surface.

3.2. Hybridization studies

The next step of the study was to examine whether hybridization of an ODN fully complementary to the PNA oligomer could be optically transduced by IR spectroscopy without external label. Indeed Mateo-Marti et al. observed a significant change of the surface IR spectrum of a SAM of PNA after hybridization of complementary DNA [33]. A drop of dA_{10} solution in PBS was spotted onto the gold-coated glass slides covered with PNA and incubated for 1 h at room temperature. After washing and drying, the gold-coated slides were again analyzed by PM-RAIRS. In the case where PNA was immobilized via the

metallocarbene strategy, a slight change of the IR spectrum was noticed with the appearance of a weak band at 1740 cm^{-1} and a broad band centered at 1100 cm^{-1} (fig. 2). The first band can only belong to the PNA since dA_{10} does not contain any C=O group. Therefore, its presence might be due to a reorientation of the PNA molecules upon hybridization with complementary DNA or to an increased rigidity of the PNA-DNA heteroduplex [26, 30, 32]. Indeed, the RAIRS technique is highly sensitive to vibrator orientation with respect to the surface. The second feature might be assigned to the symmetric mode of $\nu(PO_2^-)$ of the ODN (see fig. 2, right box). A dramatic change of the contact angle was also observed after exposure to the ODN with a decrease from 61 to 47° (Table 2). This is in agreement with the highly polar nature of DNA (compared to PNA).

In the case where PNA was immobilized via the N-hydroxysuccinimide ester strategy, exposure to complementary DNA did not yield any significant change of the IR spectrum of the gold slide (fig. 4). Therefore, the same experiment was repeated with a QCM sensor chip and frequency and dissipation were monitored during injection of dA_{10} solution in PBS (fig. 5). Relatively fast exponential decrease of the resonance frequency of the quartz sensor was immediately observed upon injection of dA_{10} which reached equilibrium in 800 s. No more change of the frequency was observed during the washing step. In parallel, the variation of dissipation was again insignificant so that frequency shift was only due to mass uptake. Therefore frequency shifts were converted into mass uptakes per area which gave a surface concentration of 48 ± 5 $ng.cm^{-2}$ = 0.94 ± 0.1 $x10^{13}$ $molecules.cm^{-2}$. On the whole, we could determine that the hybridization efficiency (=ratio of DNA density over PNA density x 100) reached nearly 90%. This relatively high ratio may be due to the absence of repulsion between PNA capture probes that is favorable to the formation of the duplexes and the relatively low coverage in PNA molecules as determined above.

The surface morphology of PNA t_{10}–DNA dA_{10} film is given in Figure 6 (A and B). Image B represents a higher resolution image of the inset indicated in Figure 6A. Surface roughness analysis was obtained from image A. Ex-situ tapping mode AFM image of the adsorbed PNA t_{10}–DNA dA_{10} film shows similar grain-like features as in the case of the PNA t_{10} films (see Figure 3), whereas roughness factor of the film is R = 1.15, which is slightly higher than for PNA t_{10} film (real surface area is 4.59 μm^2 for image A. The roughness average R_a = 11.7 ± 2.7 nm. The film thickness analysis was obtained from 44 individual height profiles, one of which is shown in Figure 6 (graph z against x) and its position is depicted as a black horizontal line in image C. Only the selected portion of the profile (white line in Figure 6C) was used for determination of the film thickness values as the height difference between the adsorbate-covered and cleaned regions. Individual film thickness values were collected and shown in Figure 6 as the height distribution histogram. Three clearly recognizable thickness values (25 ± 7 nm, 39 ± 11 nm, 54 ± 9 nm) were obtained by this method. This fact points to the existence of multilayer morphology, as previously observed for the PNA t_{10} film. The first film has a thickness of 25 nm, whereas each subsequent layer adds approximately 14 nm to the overall film thickness. The most probable thickness for the PNA t_{10}–DNA dA_{10} film is 39 ± 11 nm (see peak heights in Figure 6C), which is only slightly higher than the value observed for PNA t_{10} film thickness. This observation together with only slightly higher roughness factor for PNA t_{10}–DNA dA_{10} film provides another though indirect evidence for the occurrence of the hybridization process.

3.3. Labeling of ODN by metalcarbonyl labeling agent and hybridization study

We reasoned that hybridization of DNA to immobilized PNA might be optically transduced in the mid-IR spectral range by preliminary labeling of target DNA with a transition metalcarbonyl (TMC) reporter group. This kind of probe displays typical ν(C≡O) bands in the 2000 cm^{-1} spectral region and was already used by us to detect antigen – antibody interactions in solution or on gold-coated surfaces [56, 63, 64]. To prevent loss of target ODN recognition by the PNA, we decided to introduce the metalcarbonyl reporter at its 5'-terminus. A derivative of dA_{10} (dA_{10}-5'NH_2) to which had been appended an amino group at the 5'-terminus of the sequence was allowed to react with excess SucPentCo in basic buffer (Scheme 2). This compound is an N-hydroxysuccinimide ester that is expected to react in a site-specific fashion with the 5'-NH_2 group of the ODN.

The chromatogram of the reaction mixtures showed the presence of a new peak at t_R = 45.8 min along with the nearly complete disappearance of the peak at t_R = 28.2 min (Fig. S4). All the species present in the reaction mixtures were identified by LC-ESI-MS which also confirmed that the species at t_R = 45.8 mn was indeed dA_{10}-5'NH[$Co_2(CO)_6$] (Table S1). Based on peak areas, the degree of purity of dA_{10}-5'NH[$Co_2(CO)_6$] in the final product was ca. 60%. After removal of excess SucPentCo, the IR spectrum of dA_{10}-5'NH[$Co_2(CO)_6$] deposited on a nitrocellulose membrane displayed 3 bands at 2095, 2054 and 2027 cm^{-1} which are typical of the alkyne-[$Co_2(CO)_6$] entity (Fig. 7). ~~Quantitative analysis based on the intensity of the 2054 cm^{-1} band gave a labeling yield of 52-55 % in good agreement with the purity measured by HPLC.~~

A new film of PNA t_{10} was assembled at the surface of a gold-coated glass substrate by the metallocarbene strategy and a drop of dA_{10}-5'NH-[$Co_2(CO)_6$] in PBS was deposited on the surface. After incubation and copious washing, the surface was analyzed by PM-RAIRS. Fig. 7 shows the ν(C≡O) region of the IR spectrum of the surface before and after exposure to the labeled ODN. Before incubation, 2 bands at 2098 and 1932 cm^{-1} were observed and assigned to residual azide and aminocarbene groups, respectively. After incubation with labeled ODN, two new bands at 2052 and 2025 cm^{-1} characteristic of the $Co_2(CO)_6$ moiety appeared. Their presence could only result from the formation of PNA-DNA duplexes at the surface of the sensor.

4. Conclusions

To sum up, we have devised two strategies to generate a layer of PNA molecules at the surface of gold-coated glass / quartz sensors. Actual immobilization of PNA strands was assessed by PM-RAIRS and QCM, which also provided quantitative information on the surface coverage in PNA molecules. Subsequent hybridization of complementary ssDNA could be monitored in real time by QCM and appeared quite successful in terms of hybridization efficiency. Inability to optically transduce the formation of PNA-DNA heteroduplex by PM-RAIRS was overcome by labeling the complementary ssDNA with a transition metalcarbonyl reporter group that could then be conveniently detected thanks to the IR signature of this entity in the 2000 cm^{-1} spectral region. We now intend to set up PNA-based optical sensors to detect biologically relevant DNA sequences and study their sensitivity and specificity.

5. Acknowledgements

The Indo-French Centre for the Promotion of Advanced Research (CEFIPRA / IFCPAR) is gratefully acknowledged for financial support (project number 4105-1). The "Laboratoire de Physico-Chimie des Surfaces" of Chimie Paristech (Dr A. Galtayries) is gratefully acknowledged for the use of the IR spectrometer. S. L. thanks the COST D36 program "Molecular Structure-Performance Relationships at the Surface of Functional Materials" for financial support of short term visit to Paris. M. S. and M. H. acknowledge the CNRS - Academy of sciences of the Czech Republic exchange program. M. H. acknowledges the grant support from GACR (14-05180S). S.C. thanks the Università degli Studi di Milano for the postdoctoral fellowship. P. T. acknowledges the Università degli Studi di Milano for Ph. D. fellowship. E. L. acknowledges the CARIPLO Foundation, project 2013-0752.

6. References

[1] D. Samanta, A. Sarkar, Chem. Soc. Rev., 40 (2011) 2567-2592.
[2] A. Ulman, Chem. Rev., 96 (1996) 1533-1554.
[3] Y. Zhou, C.-W. Chiu, H. Liang, Sensors, 12 (2012) 15036-15062.
[4] M. Frasconi, F. Mazzei, T. Ferri, Anal. Bioanal. Chem., 398 (2010) 1545-1564.
[5] N.K. Chaki, K. Vijayamohanan, Biosens. Bioelectron., 17 (2002) 1-12.
[6] N.K. Devaraj, G.P. Miller, W. Ebina, B. Kakaradov, J.P. Collman, E.T. Kool, C.E.D. Chidsey, J. Am. Chem. Soc., 127 (2005) 8600-8601.
[7] A.L. Furst, M.G. Hill, J.K. Barton, Langmuir, 29 (2013) 16141-16149.
[8] Z.P. Tolstyka, W. Richardson, E. Bat, C.J. Stevens, D.P. Parra, J.K. Dozier, M.D. Distefano, B. Dunn, H.D. Maynard, Chembiochem, 14 (2013) 2464-2471.
[9] R. Chelmowski, S.D. Koester, A. Kerstan, A. Prekelt, C. Grunwald, T. Winkler, N. Metzler-Nolte, A. Terfort, C. Woell, J. Am. Chem. Soc., 130 (2008) 14952-14953.
[10] Y. Zhang, S.Z. Luo, Y.J. Tang, L. Yu, K.Y. Hou, J.P. Cheng, X.Q. Zeng, P.G. Wang, Anal. Chem., 78 (2006) 2001-2008.
[11] D. Samanta, N. Faure, F. Rondelez, A. Sarkar, Chem. Commun., (2003) 1186-1187.
[12] P. Dutta, S. Sawoo, N. Ray, O. Bouloussa, A. Sarkar, Bioconjugate Chem., 22 (2011) 1202-1209.
[13] S. Sawoo, P. Dutta, A. Chakraborty, R. Mukhopadhyay, O. Bouloussa, A. Sarkar, Chem. Commun., (2008) 5957-5959.
[14] P. Srivastava, A. Sarkar, S. Sawoo, A. Chakraborty, P. Dutta, O. Bouloussa, C. Methivier, C.M. Pradier, S. Boujday, M. Salmain, J. Organomet. Chem., 696 (2011) 1102-1107.
[15] P.E. Nielsen, M. Egholm, R.H. Berg, O. Buchardt, Science, 254 (1991) 1497-1500.
[16] V.V. Demidov, V.N. Potaman, M.D. Frank-Kamenetskil, M. Egholm, O. Buchard, S.H. Sönnichsen, P.E. Nlelsen, Biochem. Pharmacol., 48 (1994) 1310-1313.
[17] P.E. Nielsen, Curr. Op. Biotechnol., 12 (2001) 16-20.
[18] C. Briones, M. Moreno, Anal. Bioanal. Chem., 402 (2012) 3071-3089.
[19] S. Sforza, R. Corradini, T. Tedeschi, R. Marchelli, Chem. Soc. Rev., 40 (2011) 221-232.
[20] E.O. Fischer, F.R. Kreissl, J. Organomet. Chem., 35 (1972) C47-&.
[21] http://gwyddion.net.
[22] P. Wittung-Stafshede, M. Rodahl, B. Kasemo, P. Nielsen, B. Norden, Colloids Surf. A, 174 (2000) 269-273.
[23] C. Ananthanawat, T. Vilaivan, V.P. Hoven, Sens. Actuators B, 137 (2009) 215-221.
[24] M.H. Pournaghi-Azar, F. Ahour, M.S. Hejazi, Anal. Bioanal. Chem., 397 (2010) 3581-3587.

[25] N. Prabhakar, K. Arora, S.K. Arya, P.R. Solanki, M. Iwamoto, H. Singh, B.D. Malhotra, Analyst, 133 (2008) 1587-1592.
[26] H. Aoki, H. Tao, Analyst, 132 (2007) 784-791.
[27] T. Goda, A.B. Singi, Y. Maeda, A. Matsumoto, M. Torimura, H. Aoki, Y. Miyahara, Sensors, 13 (2013) 2267-2278.
[28] J.Y. Liu, L. Tiefenauer, S.J. Tian, P.E. Nielsen, W. Knoll, Anal. Chem., 78 (2006) 470-476.
[29] J.B. Raoof, R. Ojani, S.M. Golabi, E. Hamidi-Asl, M.S. Hejazi, Sens. Actuators B, 157 (2011) 195-201.
[30] S. Ghosh, R. Mukhopadhyay, J. Colloid Interface Sci., 360 (2011) 52-60.
[31] S. Ghosh, S. Mishra, R. Mukhopadhyay, Langmuir, 29 (2013) 11982-11990.
[32] E. Mateo-Marti, C. Briones, E. Roman, E. Briand, C.M. Pradier, J.A. Martin-Gago, Langmuir, 21 (2005) 9510-9517.
[33] E. Mateo-Marti, C. Briones, C.M. Pradier, J.A. Martin-Gago, Biosens. Bioelectron., 22 (2007) 1926-1932.
[34] M. Steichen, Y. Decrem, E. Godfroid, C. Buess-Herman, Biosens. Bioelectron., 22 (2007) 2237-2243.
[35] F. Hook, A. Ray, B. Norden, B. Kasemo, Langmuir, 17 (2001) 8305-8312.
[36] D.K. Corrigan, H. Schulze, G. Henihan, I. Ciani, G. Giraud, J.G. Terry, A.J. Walton, R. Pethig, P. Ghazal, J. Crain, C.J. Campbell, A.R. Mount, T.T. Bachmann, Biosens. Bioelectron., 34 (2012) 178-184.
[37] C. Yao, T. Zhu, J. Tang, R. Wu, Q. Chen, M. Chen, B. Zhang, J. Huang, W. Fu, Biosens. Bioelectron., 23 (2008) 879-885.
[38] K.K. Jensen, H. Orum, P.E. Nielsen, B. Norden, Biochemistry, 36 (1997) 5072-5077.
[39] D. Kambhampati, P.E. Nielsen, W. Knoll, Biosens. Bioelectron., 16 (2001) 1109-1118.
[40] C. Ananthanawat, T. Vilaivan, V.P. Hoven, X.D. Su, Biosens. Bioelectron., 25 (2010) 1064-1069.
[41] O. Thipmanee, S. Samanman, S. Sankoh, A. Numnuam, W. Limbut, P. Kanatharana, T. Vilaivan, P. Thavarungkul, Biosens. Bioelectron, 38 (2012) 430-435.
[42] Q. Ou, J.a. He, C. Liu, L. Shi, C. Zhao, Y. Xu, D. Gu, Biotechnol. Bioproc. Eng., 18 (2013) 1031-1037.
[43] C. Zanardi, C. Baldoli, E. Licandro, F. Terzi, R. Seeber, J. Nanoparticle Res., 14 (2012) 1148.
[44] C. Zanardi, F. Terzi, R. Seeber, C. Baldoli, E. Licandro, S. Maiorana, Artificial DNA, PNA & XNA, 3 (2012) 80-87.
[45] P. Dutta, N. Ray, S. Roy, A.K. Dasgupta, O. Bouloussa, A. Sarkar, Org. Biomol. Chem., 9 (2011) 5123-5128.
[46] E.O. Fischer, B. Heckl, H. Werner, J. Organomet. Chem., 28 (1971) 359-&.
[47] K. Weiss, E.O. Fischer, Chem. Ber., 106 (1973) 1277-1284.
[48] M. Salmain, J.C. Blais, H. Tran-Huy, C. Compain, G. Jaouen, Eur. J. Biochem., 268 (2001) 5479-5487.
[49] M. Salmain, E. Licandro, C. Baldoli, S. Maiorana, H. Tran-Huy, G. Jaouen, J. Organomet. Chem., 617 (2001) 376-382.
[50] A. Chakraborty, S. Dey, S. Sawoo, N.N. Adarsh, A. Sarkar, Organometallics, 29 (2010) 6619-6622.
[51] J.P. Collman, N.K. Devaraj, T.P.A. Eberspacher, C.E.D. Chidsey, Langmuir, 22 (2006) 2457-2464.
[52] A. Paul, R.M. Watson, P. Lund, Y. Xing, K. Burke, Y. He, E. Borguet, C. Achim, D.H. Waldeck, J. Phys. Chem. C, 112 (2008) 7233-7240.

[53] V. Kolivoska, M. Gal, M. Hromadova, S. Lachmanova, L. Pospisil, Biointerphases, 6 (2011) 164-170.
[54] V. Kolivoska, M. Gal, M. Hromadova, S. Lachmanova, H. Tarabkova, P. Janda, L. Pospisil, A. Turonova, Colloids Surf. B, 94 (2012) 213-219.
[55] A. Bonyar, G. Harsanyi, in: 34th Int. Spring seminar on Electronics Technology, ISSE, Tatranska Lomnica, Slovakia, 2011, pp. 519-524.
[56] M. Salmain, N. Fischer-Durand, C.-M. Pradier, Anal. Biochem., 373 (2008) 61-70.
[57] J. Lahiri, L. Isaacs, J. Tien, G.M. Whitesides, Anal. Chem., 71 (1999) 777-790.
[58] B. Dordi, H. Schonherr, G.J. Vancso, Langmuir, 19 (2003) 5780-5786.
[59] E. Briand, M. Salmain, C. Compere, C.-M. Pradier, Colloids Surf. B, 53 (2006) 215-224.
[60] D.Y. Petrovykh, H. Kimura-Suda, L.J. Whitman, M.J. Tarlov, J. Am. Chem. Soc., 125 (2003) 5219-5226.
[61] X.D. Su, Y.J. Wu, W. Knoll, Biosens. Bioelectron., 21 (2005) 719-726.
[62] N. Huesken, M. Gebala, F. La Mantia, W. Schuhmann, N. Metzler-Nolte, Chem. Eur. J., 17 (2011) 9678-9690.
[63] E. Briand, M. Salmain, C. Compere, C.-M. Pradier, Biosens. Bioelectron., 22 (2007) 2884-2890.
[64] C.M. Yam, C.M. Pradier, M. Salmain, N. Fischer-Durand, G. Jaouen, J. Colloid Interface Sci., 245 (2002) 204-207.

Figures captions:

Scheme 1. Immobilization of PNA via the Fischer metalloalkoxycarbene route and hybridization with complementary DNA

Scheme 2. Labeling of target ODN by a transition metalcarbonyl reporter group

Figure 1. Structure of PNA t_{10} used in the study.

Figure 2. Left box: PM-RAIRS spectra of azidoundecanethiolate SAM (A), after treatment with 1 mM metallocarbene in degassed toluene at 40°C (B), after treatment with 5 µM PNA t_{10} in borate buffer pH 8.5 (C), after treatment with 5 µM dA_{10} in PBS (D). Right box: ATR-IR spectra of PNA t_{10} and DNA dA_{10}

Figure 3. Ex-situ tapping mode AFM topography image (size 2 µm × 2 µm) of PNA t_{10} layer immobilized on the gold substrate via the Fischer metalloalkoxycarbene route.

Figure 4. PM-RAIRS analysis of gold-coated glass slides after each step of functionalization: (A) SAM of MUA; (B) after treatment with 50 mM TSTU and DIPEA in DMF; (C) after treatment with 2.4 µM PNA t_{10} in borate buffer pH 8.5; (D) after treatment with 12 µM dA_{10} in PBS

Figure 5. Left: Frequency change and mass uptake upon PNA t_{10} chemisorption on SAM of MUA activated by TSTU; a 12 µM solution of PNA t10 in carbonate buffer was flowed over the sensor for 18 min. Right: Frequency change and mass uptake upon hybridization of dA_{10}; a 12 µM solution of dA_{10} in carbonate buffer was flowed over the sensor for 15 min. The grey zones correspond to washing steps.

Figure 6. Ex-situ tapping mode AFM topography of PNA t_{10}–DNA dA_{10} layer before (A, image size 2 μm × 2 μm), (B, image size 0.5 μm × 0.5 μm) and after (C, image size 2 μm × 2 μm) removal of the film by the force of 119.7 nN. Selected height profile (black horizontal line) is shown next to the image C, together with the height distribution analysis obtained from 44 horizontally shifted profiles (indicated by a white line segment on image C).

Fig. 7. Left box: IR spectrum of dA_{10}-5'NH-$[Co_2(CO)_6]$ (5 μl of a 140 μM solution deposited on a nitrocellulose membrane); Right box: PM-RAIRS analysis of gold-coated substrates covered with a layer of PNA t_{10} (lower trace) and after exposure to 6 μM dA_{10}-5'NH-$[Co_2(CO)_6]$ in PBS (upper trace).

Tables:

Table 1 Band assignments of the surface IR spectra recorded after steps A, B, C and D

Step	Wavenumber, cm^{-1}			
	A	B	C	D
ν_{as}(C-H)	2924	2924	2924	2924
ν_{s}(C-H)	2854	2854	2854	2854
ν_{as}(N_3)	2090			
ν(C≡O) (A_1)		2067	2063	
ν(C≡O) (B_1)		1982		
ν(C≡O) (E+A_1)		1940	1932	1925
ν(C=O)				1740
ν(C=C) ν(C=O) amide I		1639 (br)	1651 (br)	1647 (br)
∂(C-H), ν(N=N)	1454	1443	1462	1454
ν_{as}(P=O)				1100 (br)

Table 2 Contact angle measurements

Step / sample	Contact angle, °
Gold	96.3 ± 0.4
Annealed gold	58.5 ± 0.7
A	70.8 ± 0.6
B	66.7 ± 0.7
C	61.5 ± 0.6
D	47.4 ± 0.4

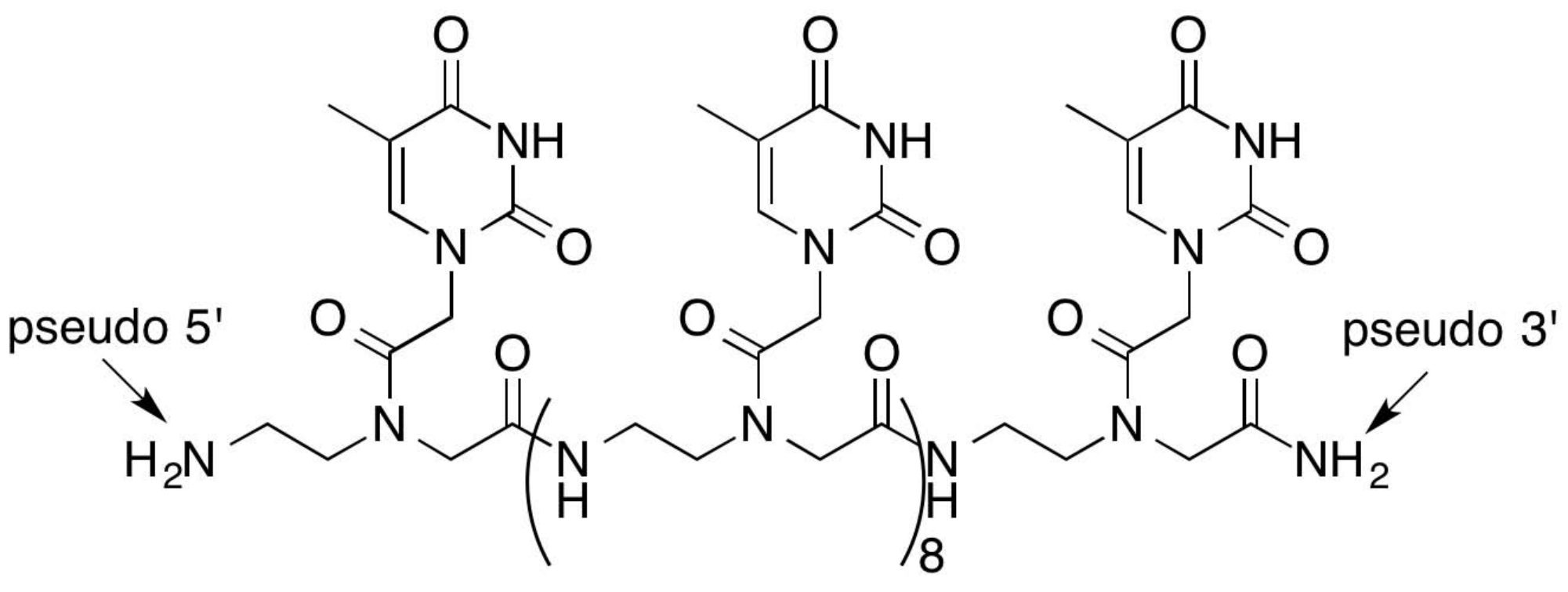
pseudo 5'
pseudo 3'
O
NH
N
O
H_2N
NH_2
8

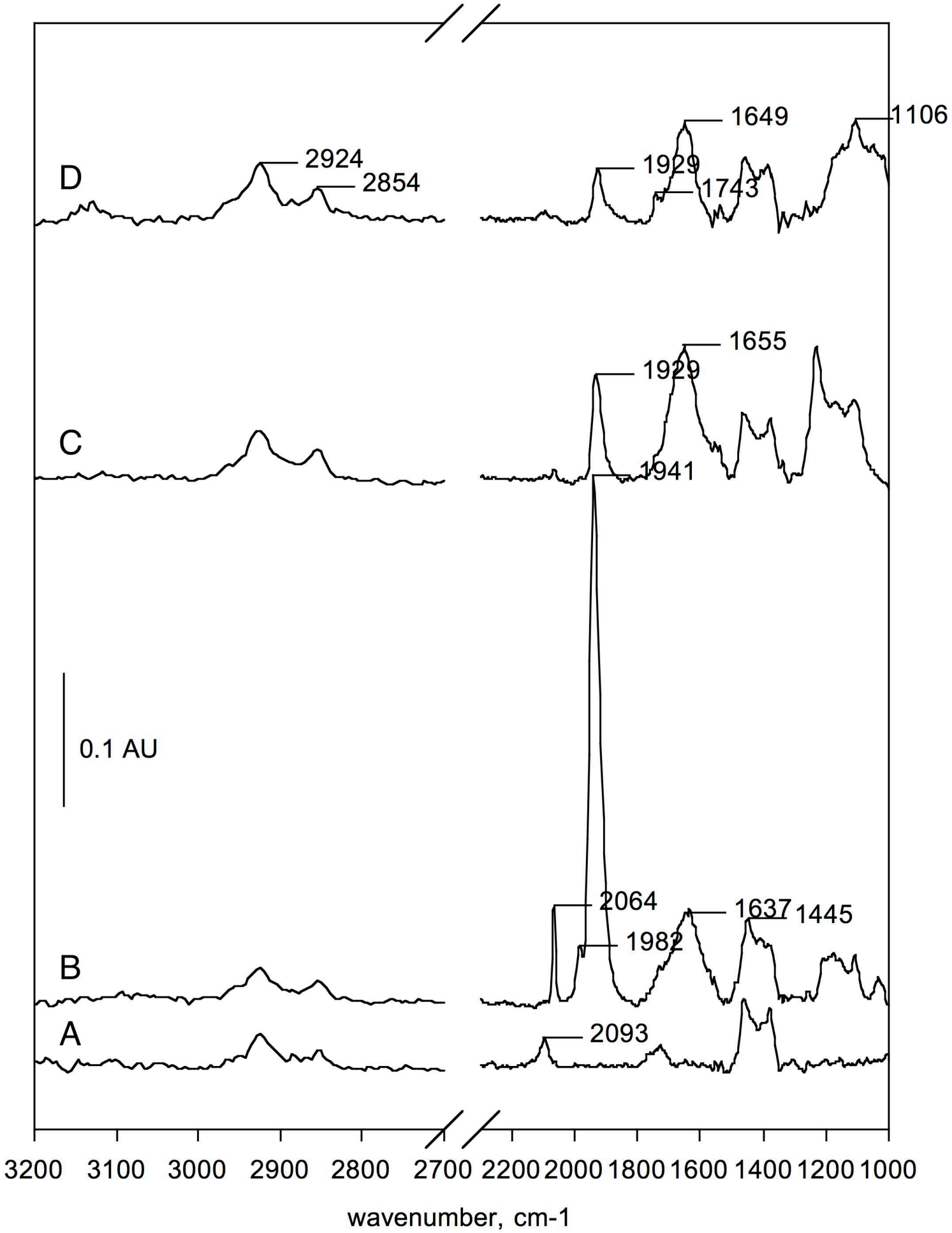
D
2924
2854
1649
1106
1929
1743
C
1655
1929
1941
0.1 AU
B
2064
1637
1445
1982
A
2093
3200 3100 3000 2900 2800 2700 2200 2000 1800 1600 1400 1200 1000
wavenumber, cm-1

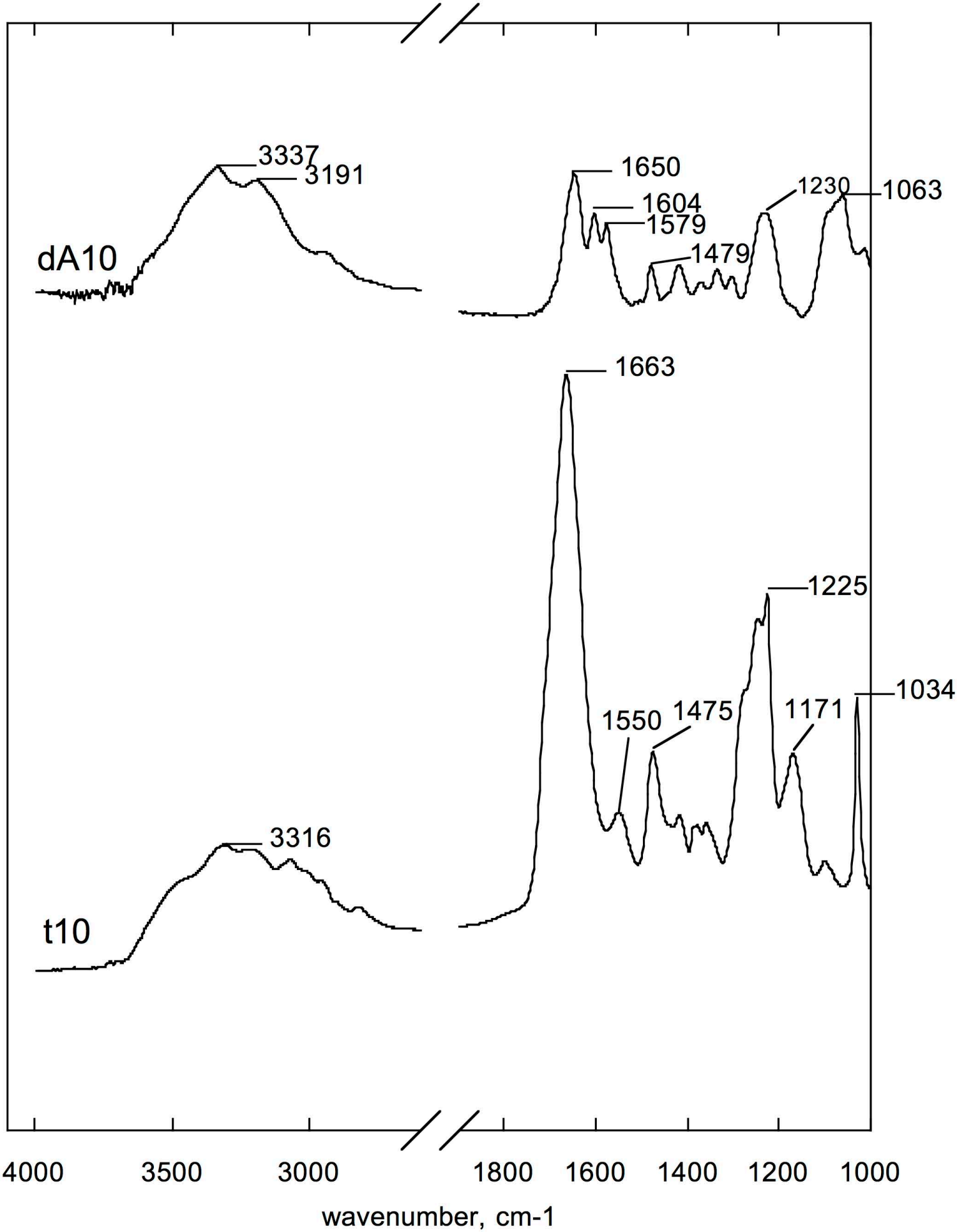
dA10
3337
3191
1650
1604
1579
1479
1230
1063
t10
3316
1663
1550
1475
1225
1171
1034
4000
3500
3000
1800
1600
1400
1200
1000
wavenumber, cm-1

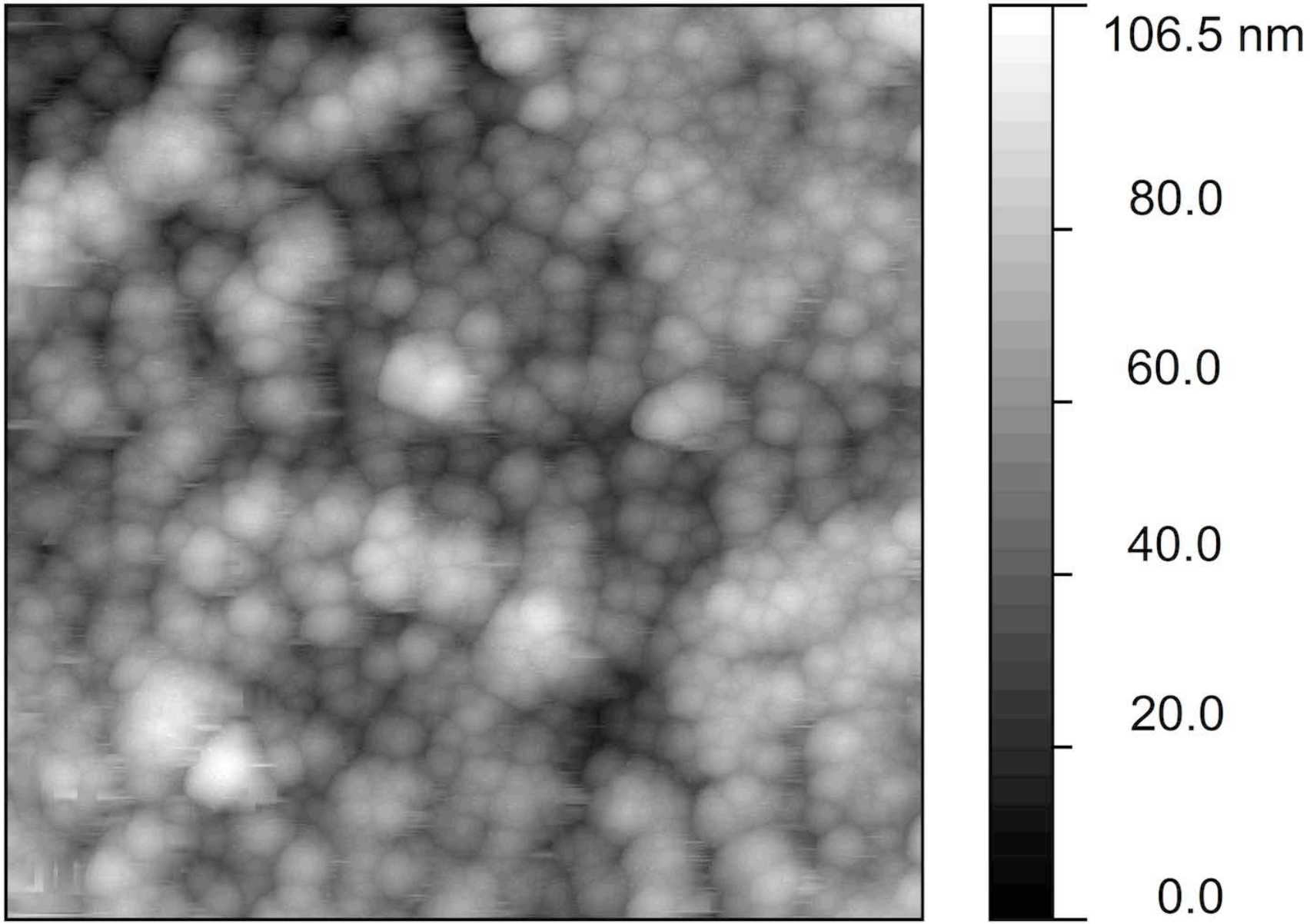
106.5 nm
80.0
60.0
40.0
20.0
0.0

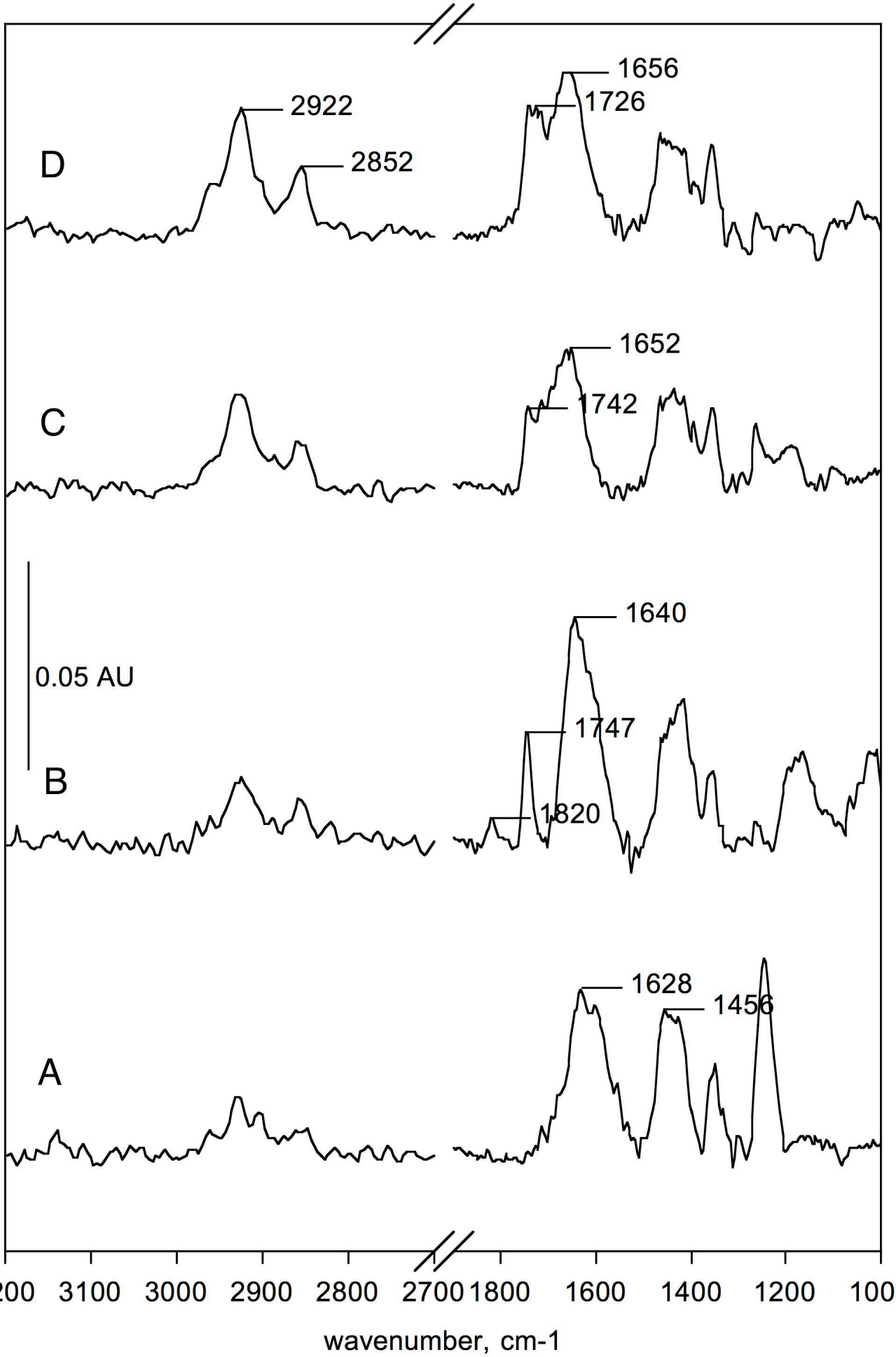
D
2922
2852
1656
1726
C
1652
1742
0.05 AU
B
1640
1747
1820
A
1628
1456
3200
3100
3000
2900
2800
2700
1800
1600
1400
1200
1000
wavenumber, cm-1

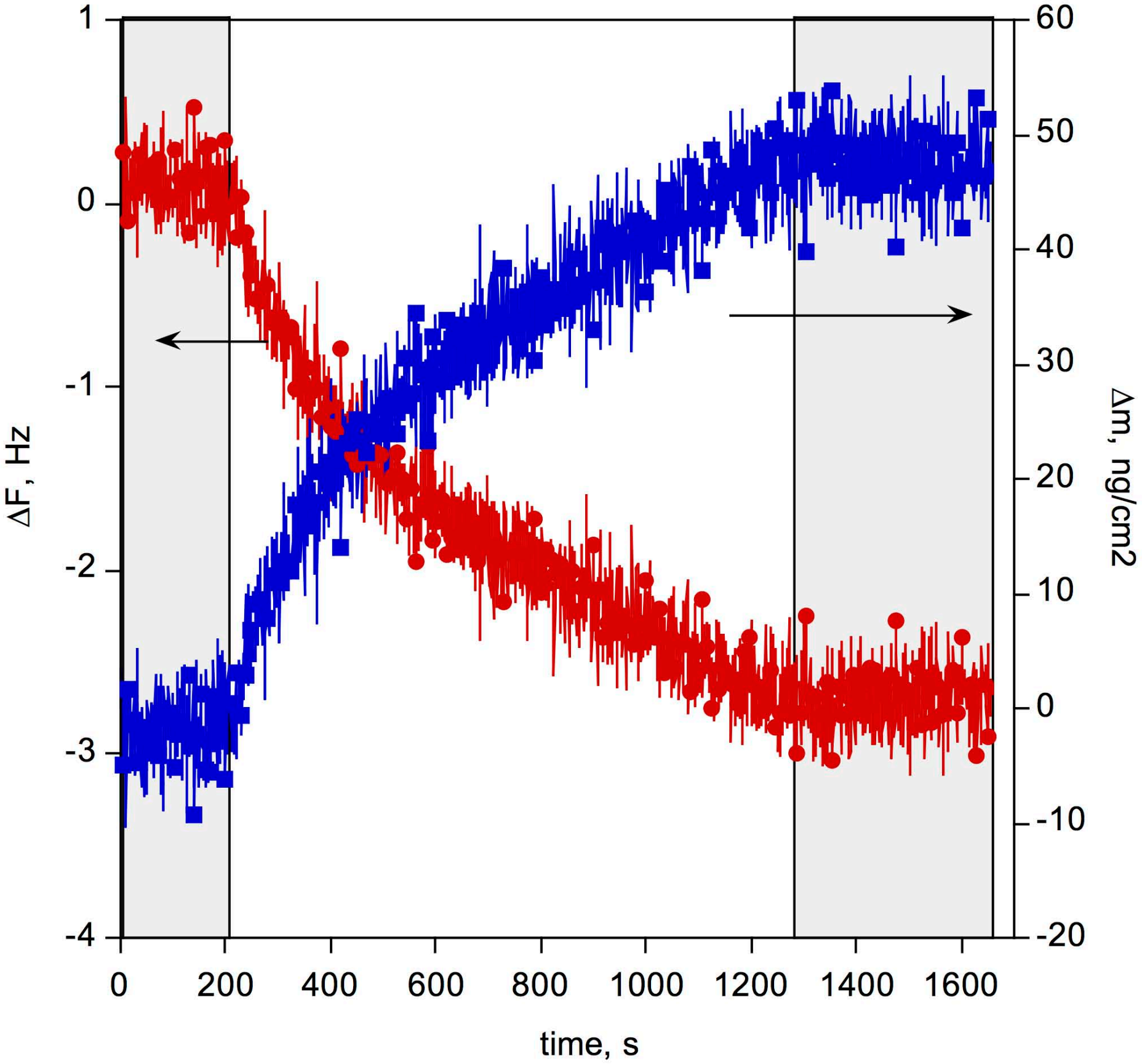
1
0
-1
-2
-3
-4
ΔF, Hz
60
50
40
30
20
10
0
-10
-20
Δm, ng/cm2
0
200
400
600
800
1000
1200
1400
1600
time, s

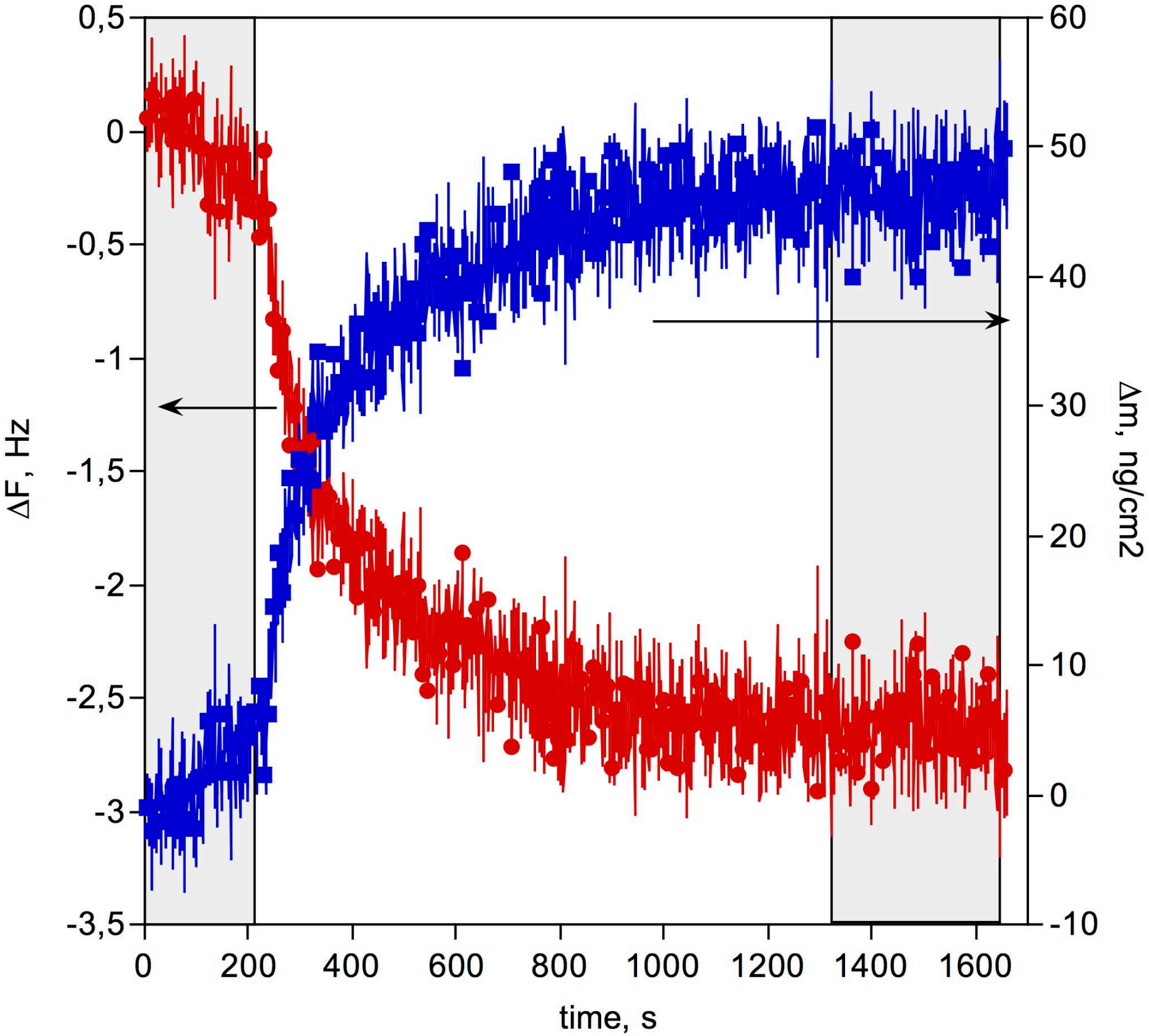
0,5
0
-0,5
-1
-1,5
-2
-2,5
-3
-3,5
ΔF, Hz
60
50
40
30
20
10
0
-10
Δm, ng/cm2
0
200
400
600
800
1000
1200
1400
1600
time, s

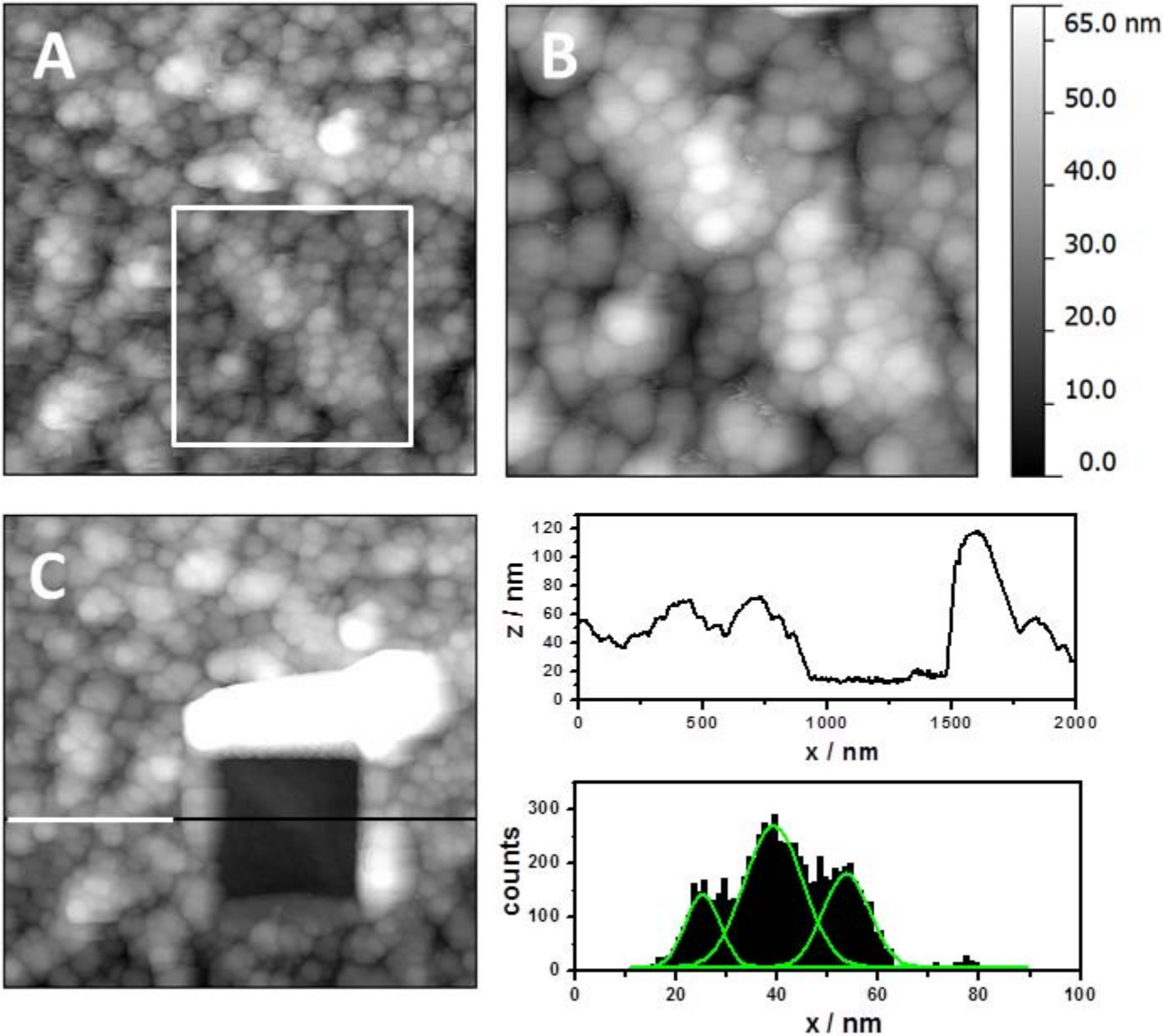
A
B
65.0 nm
50.0
40.0
30.0
20.0
10.0
0.0
C
z / nm
120
100
80
60
40
20
0
0
500
1000
1500
2000
x / nm
counts
300
200
100
0
0
20
40
60
80
100
x / nm

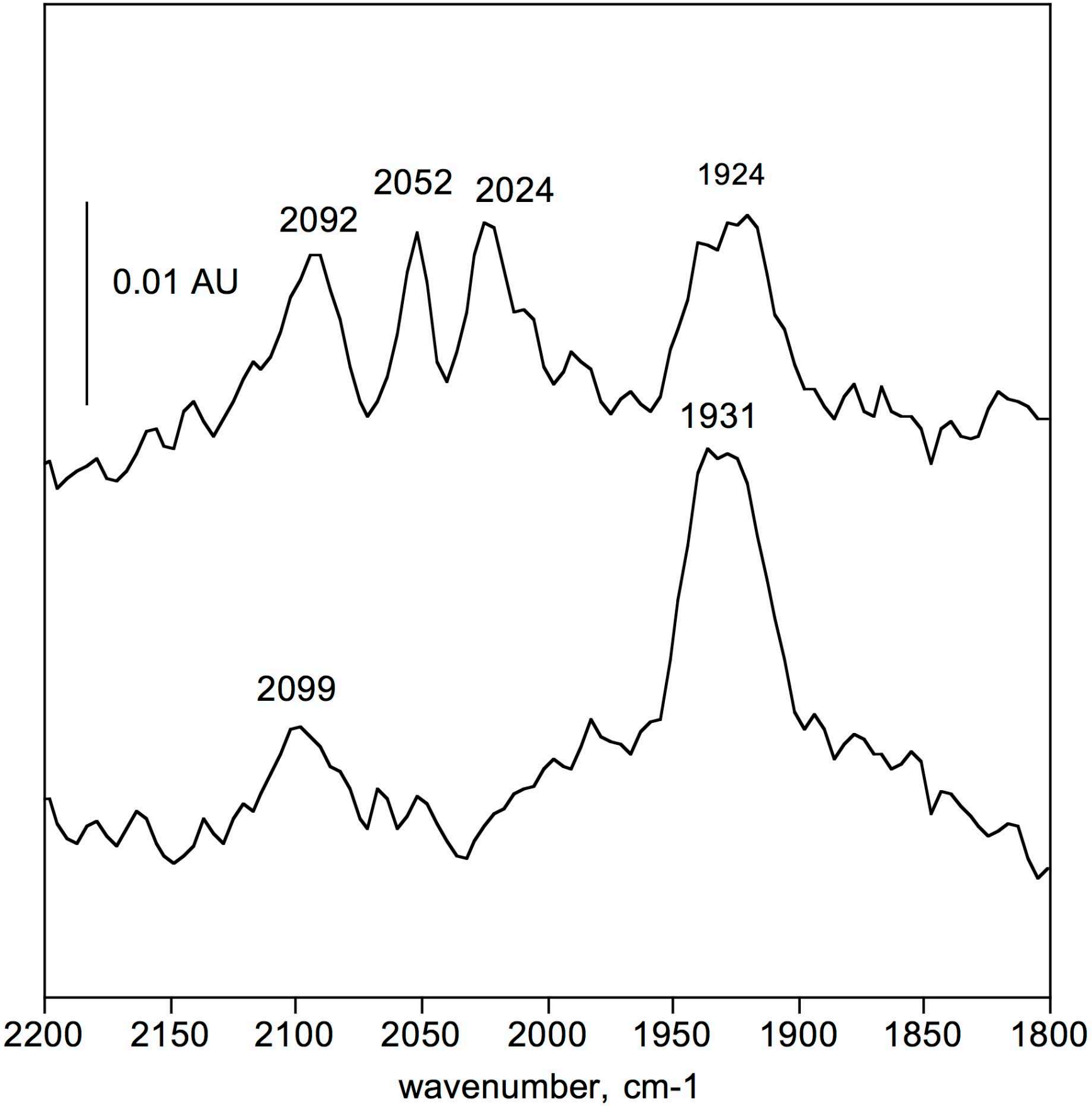
2092
2052
2024
1924
0.01 AU
1931
2099
2200
2150
2100
2050
2000
1950
1900
1850
1800
wavenumber, cm-1